Mode-Matching Analysis of Lossy SIW Devices

Massimiliano Casaletti, Guido Valerio, Ronan Sauleau, Matteo Albani

Mode-Matching Analysis of Lossy SIW Devices

Massimiliano Casaletti, *Member, IEEE*, Guido Valerio, *Member, IEEE*,
Ronan Sauleau, *Senior Member, IEEE*, and Matteo Albani, *Senior Member, IEEE*

***Abstract*— In this paper, the authors present a method for the analysis of lossy Substrate Integrated Waveguide (SIW) structures. The analysis is achieved through the cylindrical-wave mode expansion of the field and a mode matching technique to enforce boundary conditions on the post surfaces. We introduce an approximated formulation of the previous exact procedure, valid in the microwave regime, and numerically examine a number of microwave devices using both approximated and exact analyses. These devices include filters, couplers, phase shifter, etc. Results are presented for the scattering parameters and compared to those obtained with commercial software in terms of accuracy and computational time.**

***Index Terms*— conductor losses, Green's functions, method of moments (MoM), SIW**

I. Introduction

With an ever-increasing number of micro- and millimeter-wave devices being built in substrate-integrated waveguide (SIW) technology [1]-[4], and their inevitably increasing complexity (e.g., [5]-[7]), there is need for a fast and accurate method of analyzing and optimizing such devices. Moreover, with the shift of applications of this attractive technology to higher frequency bands (even as high as the D-band [8]), one needs to accurately assess conductor losses, which become the dominant loss mechanism in SIW-based devices at higher frequencies [9], significantly degrading the performance of devices, e.g., lowering the gain of slotted arrays or increasing the insertion loss of SIW-filters. This is especially important when low-cost fabrication techniques relying on low-conductivity metals are employed. In addition, the conductor roughness, especially of the ground plates, starts to play a role in the overall loss, further increasing it. This is particularly important for specific manufacturing technology as Low Temperature Co-fired Ceramic (LTCC) or low cost inkjet processes [10].

Over the past years, several methods for the analysis of SIW devices have been proposed, ranging from finite-difference schemes [11], equivalent-width waveguide methods [12], boundary integral-resonant method [13] and integral-equation-based methods [14]-[19]. However, most of these methods lack in generality, being applicable mostly to shielded PEC structures mimicking conventional rectangular waveguides [9], [17], [18], dealing with electrically thin cylindrical scatterers [14], or operating in the Transverse Magnetic (TM) mode regime [15]-[18]. This is a hindrance to designing, since one has to consider carefully the effect of all relevant modes [20]-[22], which may be induced at discontinuities in the system under consideration, and, more importantly, since the geometry may in general be irregular and quite complex. Furthermore, the losses were modeled using approximations of severely restricted validity, mostly by effective or empirically determined surface impedances as in [9] and [12]. In [16], losses were incorporated into an approximate mode-matching analysis of single-waveguide SIW structures. However, only the basic coaxial feed was used to excite the structures under study, limiting the analysis to the study of TM modes only. Moreover, the coaxial feeds were approximately modeled as magnetic currents radiating into an infinite perfectly electric conductor (PEC) parallel-plate waveguide (PPW). This may be valid when the conductivity of the ground plane is high, but when this is not the case, this approximation yields inaccurate feeding fields as the coaxial feed may induce higher-order modes in the waveguide. Also, the connecting vias were considered to be exclusively PEC, thus avoiding coupling between Transverse Electric (TE) and TM modes, which can be significant when low-conductivity metal is used.

Therefore, one needs a general, reliable and efficient analysis tool that could take into account properly the aforementioned effects and consequently be used in design and optimization. The authors have recently proposed a hybrid Method of Moments (MoM)/Mode-Matching (MM) method [21],[23], capable of accurately analyzing stacked planar SIW structures with the possible presence of coupling or radiating slots etched in conducting plates. Here we extend the *mode-matching* part, which can be subsequently used as the building block in the MoM framework (e.g., [23]), to incorporate conductor losses in a rigorous manner. The resulting code provides a reliable full-wave tool to design and optimize SIW devices by rigorously taking into account losses. A significant reduction of computation time and memory usage is achieved with respect to commercial software, especially when large structures are considered and need to be optimized.

The formulation of the problem in terms of lossy eigenfunctions is similar to the one presented in [24], where only slots in a PPW are considered in the absence of vertical posts. The formulation has been described with no mathematical details and no results in [25]. The need of non-

Manuscript received 23/03/2015; revised DATE.

The authors would like to thank the Agence Nationale de la Recherche (grant ANR 2010 VERS 001301, grant ANR 12-EMMA-0041-01) and DGCIS (FUI 10, DENOTEIC).

M. Casaletti and G. Valerio are with the Sorbonne Universités, UPMC Univ. Paris 06, UR2, L2E, F-75005, Paris, France (e-mail: massimiliano.casaletti@upmc.fr, guido.valerio@upmc.fr).

R. Sauleau is with the Institute of Electronics and Telecommunications of Rennes (IETR), UMR CNRS 6164, University of Rennes 1, 35042 Rennes, France (e-mail: ronan.sauleau@univ-rennes1.fr).

M. Albani is with the Dipartimento di Ingegneria dell'Informazione Università degli Studi di Siena, Via Roma 56, 53100, Siena, Italy (e-mail: matteo.albani@dii.unisi.it).

orthogonal vertical eigenfunctions in the presence of lossy plates has been introduced in [26], together with preliminary numerical results of a structure not shown in this paper. However, details on the actual implementation are discussed here for the first time.

To be more specific, we model both the conductor losses and small metal surface roughness using the Leontovich boundary condition [27], granting the description of lossy or rough metal surfaces as surface impedances. This allows one to derive analytically the necessary scalar Green's functions, and, subsequently, a set of scalar potentials from which the PPW dyadic admittance Green's function can be obtained through differentiation [28]. The lossy metal vias are modeled either as lossy-dielectric cylinders, or as surface impedances, whose scattered fields can be found by enforcement of the impedance boundary conditions on their respective surfaces. In addition, we consider the effect of placing a coaxial feed over a lossy plane through the application of the equivalence principle in a rigorous manner.

The paper is organized as follows. Section II gives a brief outline of the derivation of both the necessary Green's functions and the vector wave functions with special emphasis on the underlying mathematical structure.

In Section III, mode coupling in lossy SIW is quantitatively studied, while in Section IV an approximated mode-matching approach is derived, based on previous section results. Section V deals with the definition and computation of input parameters. Finally, in Section VI, we validate the results of numerical analysis by comparison against an FEM-based commercial code in terms of accuracy and computation time.

II. Mathematical Background

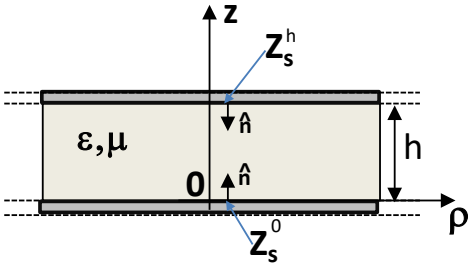

Fig. 1. Lateral view of a lossy PPW

In typical microwave applications, SIW channels are obtained by drilling commercial metalized dielectric substrates, and then filling the holes with conducting materials (or dielectric) in order to implement the cylindrical posts. This procedure leads to structures that use the same kind of metallization for both top and bottom planes. Moreover, at this frequency regime, the roughness of the metallization can be in general neglected. All these considerations lead to the use of the Leontovich equivalent boundary condition for the metallic planes

$$Z_s = (1+j)\sqrt{\omega\mu_s/(2\sigma)} \tag{1}$$

where σ is the conductivity, ω is the angular velocity and μ_s is the permeability. Other type of surfaces (such as thin metals [29], rough surfaces [30][31] or partially reflecting surfaces [32]) can be modeled through an equivalent impedance. For the sake of brevity, in this work only lossy metal plates will be considered henceforth.

The structure under analysis consists of a PPW, defined by two horizontal lossy metallic plates placed at a distance *h*, laterally unbounded, filled by a dielectric medium (see Fig. 1). Inside the PPW an arbitrary number of vertical cylindrical posts can be placed, either of penetrable or impenetrable medium.

From a computational point of view, it is of paramount importance to choose the most effective representation according to the kind of field. In this view, the cylindrical eigenmode expansion of the field seems to be the appropriate choice [33]. The fields scattered by these posts can be modeled by linear sums of vector modes with unknown amplitude, while the incident field on the posts can be computed through a Green's function represented in terms of eigenfunctions expansion [33]. The scattered amplitudes are then found by imposing boundary conditions on the post surfaces.

Vector functions are defined as in [30, Sec. 7.2]

$$\begin{aligned}\mathbf{M}(\mathbf{r}) &= \nabla\times\left[\hat{\mathbf{z}}\Phi^{TM}(\mathbf{r})\right],\\ \mathbf{N}(\mathbf{r}) &= \frac{1}{k}\nabla\times\nabla\times\left[\hat{\mathbf{z}}\Phi^{TE}(\mathbf{r})\right],\end{aligned} \tag{2}$$

referring to the transverse (with respect to *z*) magnetic field TM^z and TE^z polarization, respectively. The scalar Φ functions must satisfy the scalar Helmholtz equation.

Assuming a $e^{j\omega t}$ time harmonic dependence, it can be solved by conventional means, through separation of variables in cylindrical coordinates $\mathbf{r}\equiv(\rho,\phi,z)$ (in anticipation of the presence of circular cylindrical scatterers), yielding

$$\Phi^t_{mn}(\mathbf{r}) = c_m\begin{bmatrix} J_n\left(k^t_{\rho_m}\rho\right)\\ H^{(2)}_n\left(k^t_{\rho_m}\rho\right)\end{bmatrix}e^{-jn\phi}\psi^t_m(z), \tag{3}$$

with $t=$ TM/TE, where J_n and $H^{(2)}_n$ are *n*-th order Bessel and second kind Hankel functions describing the radial dependence of fields inside and outside the posts, respectively. $k^t_{\rho_m}$, $k^t_{z_m}$ are the *m*-th TM/TE mode transverse propagation constants and the *z* functions are eigenvalues of the Sturm-Liouville problem

$$\left[\frac{d^2}{dz^2}+\left(k^t_z\right)^2\right]\psi^t(z)=0 \tag{4}$$

subject to the following boundary conditions on the conductor plates

$$\left[j\omega\varepsilon Z_s - \left(\hat{\mathbf{n}}\cdot\hat{\mathbf{z}}\right)\frac{d}{dz}\right]\psi^{TM}\left(z\right)\Big|_{z=0,h} = 0,$$
$$\left[1-\left(\hat{\mathbf{n}}\cdot\hat{\mathbf{z}}\right)\frac{Z_s}{j\omega\mu}\frac{d}{dz}\right]\psi^{TE}\left(z\right)\Big|_{z=0,h} = 0. \quad (5)$$

Since the coefficients of the terms in the boundary conditions are complex, this defines a nonself-adjoint Sturm-Liouville problem [30, Sec. 5.3]. If we wish to construct complete orthonormal sets based on these solutions in order to construct arbitrary fields, we need *normalized* eigenfunctions. This can be accomplished through a suitable choice of the coefficients c_m. Using the L^2-Hermitian inner product the eigenfunctions $\overline{\psi}$ of the adjoint problem are obtained from a Helmholtz operator having a complex conjugate wavenumber and adjoint boundary conditions at the conducting plates.

Since the solutions $\overline{\psi}$ to the adjoint TM/TE problems are the complex conjugate of ψ, the normalization can be performed through the bi-orthogonality relationship as [22, Sec. 5.3]

$$\left\langle \psi_m^t, \overline{\psi}_n^t \right\rangle = \int_0^h \psi_m^t\left(z\right)\overline{\psi}_n^{t*}\left(z\right)dz = \delta_{mn}, \quad (6)$$

with $t = \text{TM/TE}$ and δ_{mn} denoting the Kronecker's symbol $\delta_{mn}=1$ when $m=n$ or $\delta_{mn}=0$ when $m\neq n$.

This procedure leads to

$$\psi_m^{TM} = \overline{\psi}_m^{TM*} = \sqrt{\frac{2}{h}}\frac{Z_m^{TM}\cos\left(k_{z_m}^{TM}z\right)+jZ_s\sin\left(k_{z_m}^{TM}z\right)}{\sqrt{\left(Z_m^{TM}\right)^2 - Z_s^2 + 2jZ_m^{TM}Z_s\Big/\left(k_{z_m}^{TM}h\right)}},$$
$$\psi_m^{TE} = \overline{\psi}_m^{TE*} = \sqrt{\frac{2}{h}}\frac{Z_m^{TE}\sin\left(k_{z_m}^{TE}z\right)-jZ_s\cos\left(k_{z_m}^{TE}z\right)}{\sqrt{\left(Z_m^{TE}\right)^2 - Z_s^2 - 2jZ_m^{TE}Z_s\Big/\left(k_{z_m}^{TE}h\right)}}. \quad (7)$$

where $Z_m^{TM} = \dfrac{k_{z_m}^{TM}}{\omega\varepsilon}, Z_m^{TE} = \dfrac{\omega\mu}{k_{z_m}^{TE}}$ are the modal impedance of the m-th TM/TE mode, respectively and $k_{z_m}^{TM}, k_{z_m}^{TE}$ are the m-th solution (eigenvalues) of the following dispersion equations

$$j\left(Z_s^2 + Z_m^{TM^2}\right)\tan\left(k_{z_m}^{TM}z\right) + 2Z_m^{TM}Z_s = 0$$
$$j\left(Z_s^2 + Z_m^{TE^2}\right)\tan\left(k_{z_m}^{TE}z\right) + 2Z_m^{TE}Z_s = 0 \quad (8)$$

The field scattered by the posts in the whole SIW structure is thus expressed as a discrete sum of vector cylindrical waves defined as

$$\mathbf{H}_s\left(\mathbf{r}\right) = \sum_{l=1}^{N_{\text{post}}}\sum_{m=1}^{+\infty}\sum_{n=-\infty}^{+\infty}\Big[A_{mnl}^{TM}\mathbf{M}_n\left(k_{\rho_m}^{TM}, k_{z_m}^{TM}, \boldsymbol{\rho}-\boldsymbol{\rho}_l, z\right) + A_{mnl}^{TE}\mathbf{N}_n\left(k_{\rho_m}^{TE}, k_{z_m}^{TM}, \boldsymbol{\rho}-\boldsymbol{\rho}_l, z\right)\Big] \quad (9)$$

where, for the vector eigenfunctions (2) the Bessel function J_n is used for the field inside the posts, while the second kind Hankel function $H_n^{(2)}$ is used elsewhere.

Having obtained orthonormal bases for the eigenfunction expansion, we proceed to derive the dyadic magnetic Green's function, given in [28],[24] as

$$\underline{\mathbf{G}}^{PPW,HM}\left(\mathbf{r},\mathbf{r}'\right) = -\frac{1}{k^2}\left[\hat{\mathbf{z}}\hat{\mathbf{z}} + \frac{\nabla_t\nabla_t}{\nabla_t^2}\right]\delta\left(\mathbf{r}-\mathbf{r}'\right) + \frac{1}{4j}\times$$
$$\sum_{m=0}^{+\infty}\sum_{n=-\infty}^{\infty}\frac{\left(-1\right)^n}{k_{\rho_m}^{TM^2}}\mathbf{M}_{m,-n}\left(k_{\rho_m}^{TM}, k_{z_m}^{TM}, \boldsymbol{\rho}', z'\right)\mathbf{M}_{mn}\left(k_{\rho_m}^{TM}, k_{z_m}^{TM}, \boldsymbol{\rho}, z\right) \quad (10)$$
$$+\sum_{m=1}^{+\infty}\sum_{n=-\infty}^{\infty}\frac{\left(-1\right)^n}{k_{\rho_m}^{TE^2}}\mathbf{N}_{m,-n}\left(k_{\rho_m}^{TE}, k_{z_m}^{TE}, \boldsymbol{\rho}', z'\right)\mathbf{N}_{mn}\left(k_{\rho_m}^{TE}, k_{z_m}^{TE}, \boldsymbol{\rho}, z\right)$$

Thus, the incident magnetic field radiated by a magnetic source $\mathbf{J}_M$ distributed on a surface S' is obtained as the convolution of (10) with $\mathbf{J}_M$, resulting in

$$\mathbf{H}^{PPW}\left(\mathbf{r},\mathbf{r}'\right) = \sum_{m=0}^{+\infty}\sum_{n=-\infty}^{\infty}v_{m,-n}^{TM}\mathbf{M}_{mn}\left(k_{\rho_m}^{TM}, k_{z_m}^{TM}, \boldsymbol{\rho}', z'\right) + \sum_{m=1}^{+\infty}\sum_{n=-\infty}^{\infty}v_{m,-n}^{TE}\mathbf{N}_{mn}\left(k_{\rho_m}^{TE}, k_{z_m}^{TE}, \boldsymbol{\rho}', z'\right) \quad (11)$$

where

$$v_{mn}^t = -\frac{\omega\varepsilon_0\varepsilon_r\left(-1\right)^n}{4\left(k_{\rho_m}^t\right)^2}\int_{S'}\mathbf{P}_{mn}^t\left(k_{\rho_m}^t, k_{z_m}^t, \boldsymbol{\rho}'-\boldsymbol{\rho}_q, z'\right)\cdot\mathbf{J}_M\left(\mathbf{r}'\right)d^2r', \quad (12)$$

with $\mathbf{P}_{mn}^{TM} = \mathbf{M}_{mn}$, $\mathbf{P}_{mn}^{TE} = \mathbf{N}_{mn}$.

For a given source, the expansion coefficients for the field are found through a MM procedure by imposing boundary conditions on the post surfaces, as explained in next Section.

III. Determination of the Coefficients of the Scattered Field Expansion

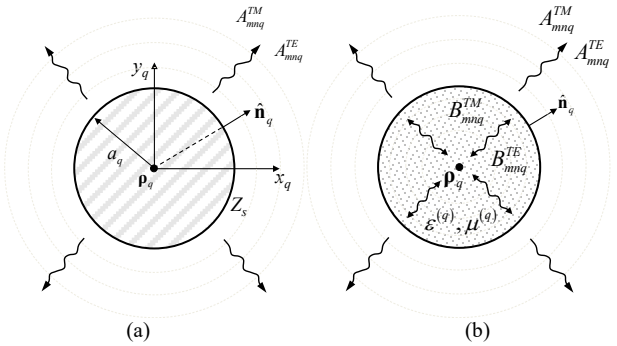

Fig. 2. Vector eigenfunction expansion of the scattered field from: (a) impenetrable post; (b) penetrable post.

Once the dyadic Green's function and vector wave functions are known, one can proceed to the formulation of the MM/MoM problem, since all types of fields (impressed and scattered) on the post surfaces can be described efficiently. A resolvable system of linear equations is obtained by imposing

the appropriate boundary conditions.

A. *Impenetrable posts*

To determine the field scattered by an impenetrable post (Fig. 2a) of radius a_q, described by a non-dispersive impedance condition Z_s, we impose the following boundary condition on the surface of the post

$$\hat{\boldsymbol{\rho}}_q \times \mathbf{E}^{\mathrm{TOT}}(\mathbf{r})\big|_{|\boldsymbol{\rho}-\boldsymbol{\rho}'|=a_q} = Z_s \hat{\boldsymbol{\rho}}_q \times \hat{\boldsymbol{\rho}}_q \times \mathbf{H}^{\mathrm{TOT}}(\mathbf{r})\big|_{|\boldsymbol{\rho}-\boldsymbol{\rho}'|=a_q} \quad (13)$$

where $\hat{\boldsymbol{\rho}}_q$ is the radial unit vector directed from the center of the post toward the exterior of the post, and $\mathbf{E}^{\mathrm{TOT}}$ and $\mathbf{H}^{\mathrm{TOT}}$ are the total electric and magnetic fields, respectively. For $Z_s = 0$ condition (13) resort to the PEC post case.

The fields are expanded through cylindrical wave functions as in (9). From the two scalar components of the vector identity (13) a couple of linear equations is obtained for the unknowns A^t_{mnq}. They are expressed as a series of azimuthal modes with linear phase around the q-th cylinder. From the orthogonality of the azimuthal eigenfunctions $e^{jn\phi}$ (see [21]) we can obtain two linear equations for each azimuthal harmonic $\bar{n}$

$$f_\phi^{\bar{n}}\left(A^{TM}_{mnq}, A^{TE}_{mnq}\right) = t_\phi^{\bar{n}}, \quad f_z^{\bar{n}}\left(A^{TM}_{mnq}, A^{TE}_{mnq}\right) = t_z^{\bar{n}} \quad (14)$$

The two equations come from the ϕ and the z components of (13); $f_\phi^{\bar{n}}$ and $f_z^{\bar{n}}$ are linear functions of A^{TM}_{mnq} and A^{TE}_{mnq}, $t_\phi^{\bar{n}}$ and $t_z^{\bar{n}}$ are known quantities depending on the excitation current. For each harmonic $\bar{n}$, (14) can then be projected on the $\bar{m}$-th adjoint vertical eigenfunction $\bar{\Psi}^t_{\bar{m}}$ in order to obtain a linear system having the same number of equations and unknowns. The obtained equations contains the scalar products between different polarization eigenfunctions: $\left\langle \Psi^{TE\prime}_m, \bar{\Psi}^{TM}_{\bar{m}} \right\rangle, \left\langle \Psi^{TM\prime}_m, \bar{\Psi}^{TE}_{\bar{m}} \right\rangle$.

If $Z_s = 0$, (13) and (14) both reduce to the simpler case of a PEC post, where the TE and TM polarizations are decoupled.

B. *Penetrable posts*

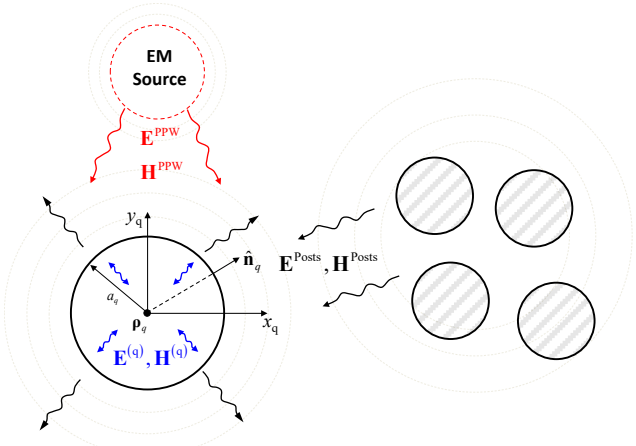

Fig. 3. Incident scattered and transmitted field in a penetrable post.

To determine the field scattered from a penetrable (possibly lossy) post, whose radius is a_q and complex dielectric constants are $\varepsilon_r^{(q)}, \mu_r^{(q)}$, the continuity of the tangential electric and magnetic fields are imposed on the post surface (Fig. 3)

$$\hat{\boldsymbol{\rho}}_q \times \mathbf{E}^{\mathrm{PPW}}(\mathbf{r}) + \hat{\boldsymbol{\rho}}_q \times \mathbf{E}^{\mathrm{Posts}}(\mathbf{r})\big|_{|\boldsymbol{\rho}-\boldsymbol{\rho}'|=a_q} = \hat{\boldsymbol{\rho}}_q \times \mathbf{E}^{(q)}(\mathbf{r})\big|_{|\boldsymbol{\rho}-\boldsymbol{\rho}'|=a_q} \quad (15)$$

$$\hat{\boldsymbol{\rho}}_q \times \mathbf{H}^{\mathrm{PPW}}(\mathbf{r}) + \hat{\boldsymbol{\rho}}_q \times \mathbf{H}^{\mathrm{Posts}}(\mathbf{r})\big|_{|\boldsymbol{\rho}-\boldsymbol{\rho}'|=a_q} = \hat{\boldsymbol{\rho}}_q \times \mathbf{H}^{(q)}(\mathbf{r})\big|_{|\boldsymbol{\rho}-\boldsymbol{\rho}'|=a_q} \quad (16)$$

where the superscripts 'PPW', 'Posts', and 'q' stand respectively for the fields excited in the PPW in the absence of the posts, for the fields scattered by all the posts, and for the field inside the q-th post under analysis. The fields in the waveguide are expanded through the Hankel function formulation of (9), while the field inside each cylinder is expanded through the Bessel function expression. Note that, if the post is metallic, a null field is retained inside the post, and only the electric field continuity (15) is used.

Each equation (15)-(16) can be projected along the ϕ and the z directions, thus obtaining a system of four scalar equations for the unknown coefficient $A^{TM/TE}_{mnl}$ and $B^{TM/TE}_{mnl}$. These scalar equations are then projected on the basis of harmonic functions describing the azimuthal dependence of field around the considered cylinder. For each harmonic $\bar{n}$, the two equations resulting from the components of (15) are

$$e_\phi^{\bar{n}}\left(A^{TM}_{mnl}, B^{TM}_{mnl}\right) = t_\phi^{\bar{n}} \quad (17)$$

$$e_z^{\bar{n}}\left(A^{TM}_{mnl}, A^{TE}_{mnl}, B^{TM}_{mnl}, B^{TE}_{mnl}\right) = t_z^{\bar{n}} \quad (18)$$

and the two equations resulting from the components of (16) are

$$h_\phi^{\bar{n}}\left(A^{TE}_{mnl}, B^{TE}_{mnl}\right) = s_\phi^{\bar{n}} \quad (19)$$

$$h_z^{\bar{n}}\left(A^{TM}_{mnl}, A^{TE}_{mnl}, B^{TM}_{mnl}, B^{TE}_{mnl}\right) = s_z^{\bar{n}} \quad (20)$$

where e and h are linear functions of $A^{TM/TE}_{mnl}$ and $B^{TM/TE}_{mnl}$, and t and s are known quantities depending on the excitation current. The four equations can then be projected on the vertical eigenfunctions $\bar{\Psi}$ in order to obtain a linear system having the same number of equations and unknowns.

Specifically, a careful choice of the eigenfunctions should be done in order to obtain stable solutions even for large losses in the cylinder. In fact, we can have eigenfunctions defined *inside* the q-th post (where wavenumbers are referred to the post dielectric), namely $\bar{\Psi}^{(q)}_m$, and eigenvalues defined in the PPW (where wavenumbers are referred to the PPW dielectric), namely $\bar{\Psi}_m$. It turns out that the best strategy is to project (17) and (19) on $\bar{\Psi}_m$, and (18) and (19) on $\bar{\Psi}^{(q)}_m$

$$\left\langle e_\phi^{\bar{n}}\left(A^{TM}_{mnl}, B^{TM}_{mnl}\right), \bar{\Psi}^{TM}_{\bar{m}_1} \right\rangle = \left\langle t_\phi^{\bar{n}}, \bar{\Psi}^{TM}_{\bar{m}_1} \right\rangle \quad (21)$$

$$\left\langle h_{\phi}^{\bar{n}}\left(A_{mnl}^{TE},B_{mnl}^{TE}\right),\bar{\Psi}_{\bar{m}_2}^{TE}\right\rangle=\left\langle s_{\phi}^{\bar{n}},\bar{\Psi}_{\bar{m}_2}^{TE}\right\rangle \quad (22)$$

$$\left\langle e_{z}^{\bar{n}}\left(A_{mnl}^{TM},A_{mnl}^{TE},B_{mnl}^{TM},B_{mnl}^{TE}\right),\bar{\Psi}_{\bar{m}_2}^{TE(q)}\right\rangle=\left\langle t_{z}^{\bar{n}},\bar{\Psi}_{\bar{m}_2}^{TE(q)}\right\rangle \quad (23)$$

$$\left\langle h_{z}^{\bar{n}}\left(A_{mnl}^{TM},A_{mnl}^{TE},B_{mnl}^{TM},B_{mnl}^{TE}\right),\bar{\Psi}_{\bar{m}_1}^{TM(q)}\right\rangle=\left\langle s_{z}^{\bar{n}},\bar{\Psi}_{\bar{m}_1}^{TM(q)}\right\rangle \quad (24)$$

We can derive explicit expressions for B_{mnl}^{TM} from (21) and for B_{mnl}^{TE} from (22), and substitute them into (23) and(24). Using the bi-orthogonality relationship (6) we finally obtain two scalar equations for the unknowns A_{mnl}^{TM} and A_{mnl}^{TE}. It turns out that with the above-mentioned testing choice, these expressions are composed only by terms having ratio of Bessel/Hankel functions of eigenvalue of the same medium. Thus, also with a large imaginary part of the argument the terms remain numerically stables.

In order to enforce (21)-(24), the computation of the following scalar products is required

$$\begin{aligned}&\left\langle \psi_{m}^{TE\prime},\bar{\Psi}_{\bar{m}_1}^{TM}\right\rangle,\quad \left\langle \psi_{m}^{TM\prime},\bar{\Psi}_{\bar{m}_2}^{TE}\right\rangle,\quad \left\langle \psi_{w}^{TM},\bar{\Psi}_{\bar{m}_1}^{TM(q)}\right\rangle,\\ &\left\langle \psi_{w}^{TE},\bar{\Psi}_{\bar{m}_2}^{TE(q)}\right\rangle,\quad \left\langle \psi_{w}^{TE(q)\prime},\bar{\Psi}_{\bar{m}_1}^{TM}\right\rangle,\quad \left\langle \psi_{w}^{TM(q)\prime},\bar{\Psi}_{\bar{m}_2}^{TE}\right\rangle,\end{aligned} \quad (25)$$

where ψ_m is the *m*-th TM or TE vertical eigenfunction in the dielectric substrate, while $\psi_m^{(q)}$ is the eigenfunction relative to the *q*-th dielectric post.

IV. Approximated MM Formulation

In this section we use an approximation of (25) in order to simplify the MM procedure developed in the previous section.

Starting form analytical expressions (7), these products can be calculated rigorously in closed form and approximated as a series expansion for good conductive PPW walls.

In standard microwave applications, good conductors are characterized by small values of the ratio R_s/η, where $R_s=\sqrt{\omega\mu_s/(2\sigma)}$ and $\eta=\sqrt{\mu/\varepsilon}$. Under this hypothesis, the wavenumbers solution of (8) can be approximated as in [24]

$$\begin{aligned}k_{z_0}^{TM}&=(R_s/\eta)^{\frac{1}{2}}\sqrt{2\omega e^{j\frac{3}{4}\pi}\sqrt{2\varepsilon\mu}/h}\\ k_{z_m}^{TM}&=m\pi/h+2(R_s/\eta)e^{j\frac{3}{4}\pi}\sqrt{2\varepsilon\mu}\,\frac{\omega}{m\pi}\quad m=1,2,\ldots\\ k_{z_n}^{TE}&=n\pi/h+2(R_s/\eta)e^{j\frac{3}{4}\pi}\sqrt{\frac{2}{\varepsilon\mu}}\,\frac{n\pi}{h^2\omega}\quad n=1,2,\ldots\end{aligned} \quad (26)$$

Using (26) in the inner products (25) asymptotic expressions can be obtained for the coupling between different PPW modes for small values of R_s/η.

$$\begin{aligned}\left\langle \psi_{m}^{TM\prime},\bar{\Psi}_{n}^{TE}\right\rangle&=\delta_{mn}+\alpha(R_s/\eta)\Delta_{m,n}^{TM',TE}+O\left[(R_s/\eta)^2\right]\\ \left\langle \psi_{n}^{TE\prime},\bar{\Psi}_{m}^{TM}\right\rangle&=-\delta_{mn}+\alpha(R_s/\eta)\Delta_{m,n}^{TM,TE\prime}+O\left[(R_s/\eta)^2\right]\\ \left\langle \psi_{m}^{TM},\bar{\Psi}_{n}^{TM(q)}\right\rangle&=\delta_{mn}+\alpha(R_s/\eta)\Delta_{m,n}^{TM,TM}+O\left[(R_s/\eta)^2\right]\\ \left\langle \psi_{m}^{TE},\bar{\Psi}_{n}^{TE(q)}\right\rangle&=\delta_{mn}+\alpha(R_s/\eta)\Delta_{m,n}^{TE,TE}+O\left[(R_s/\eta)^2\right]\end{aligned} \quad (27)$$

where $\alpha=\sqrt{2\mu/\varepsilon}e^{j\frac{3}{4}\pi}$ and the amplitudes $\Delta_{m,n}$ depend on physical and geometrical parameters as shown in the appendix. For microwave applications the scalar products (25) can be safely approximated by the first terms of (27). In other words, (27) states that for typical microwave applications the scalar wavefunctions ψ_m^t of lossy SIW have the same properties as for the case of a lossless SIW. This means that the wave-vectors defined by (7) are *quasi*-orthogonal.

A. Impenetrable posts

The field scattered by an impenetrable post of radius a_q, described by a non-dispersive impedance condition Z_s under the assumption (27) has to verify on the surface the following conditions for every couple of indexes $(\bar{m},\bar{n})$

$$\begin{aligned}&\bar{n}k_{z_{\bar{m}}}^{TM}J_r\left(k_{\rho_{\bar{m}}}^{TM}a_q\right)\sum_{l=1,l\neq l_q}^{N_{post}}\sum_{n=-\infty}^{+\infty}A_{\bar{m}nl}^{TM}H_{n-\bar{n}}^{(2)}\left(k_{\rho_{\bar{m}}}^{TM}a_q\right)e^{-j(n-\bar{n})\phi_{lq}}\\ &+\bar{n}A_{\bar{m}\bar{n}q}^{TM}k_{z_{\bar{m}}}^{TM}H_{\bar{n}}^{(2)}\left(k_{\rho_{\bar{m}}}^{TM}a_q\right)\\ &+a_q\left[jkk_{\rho_{\bar{m}}}^{TE}J_{\bar{n}}'\left(k_{\rho_{\bar{m}}}^{TE}a_q\right)+\vartheta k_{\rho_{\bar{m}}}^{TE^2}J_{\bar{n}}\left(k_{\rho_{\bar{m}}}^{TE}a_q\right)\right]\times\\ &\sum_{l=1,l\neq q}^{N_{post}}\sum_{n=-\infty}^{+\infty}A_{\bar{m}nl}^{TE}H_{n-\bar{n}}^{(2)}\left(k_{\rho_{\bar{m}}}^{TE}\left|\boldsymbol{\rho}_q-\boldsymbol{\rho}_l\right|\right)e^{-j(n-\bar{n})\phi_{lq}}\\ &+A_{\bar{m}\bar{n}q}^{TE}a_q\left[jkk_{\rho_m}^{TE}H_{\bar{n}}^{(2)\prime}\left(k_{\rho_m}^{TE}a_q\right)+\vartheta k_{\rho_{\bar{m}}}^{TE^2}H_{\bar{n}}^{(2)}\left(k_{\rho_{\bar{m}}}^{TE}a_q\right)\right]\\ &=v_{\bar{m},-\bar{n}}^{TE}a_q\left[-\vartheta k_{\rho_{\bar{m}}}^{TE^2}J_{\bar{n}}\left(k_{\rho_{\bar{m}}}^{TE}a_q\right)-jkk_{\rho_{\bar{m}}}^{TE}J_{\bar{n}}'\left(k_{\rho_{\bar{m}}}^{TE}a_q\right)\right]\\ &-\bar{n}v_{\bar{m},-\bar{n}}^{TM}k_{z_{\bar{m}}}^{TM}J_{\bar{n}}\left(k_{\rho_{\bar{m}}}^{TM}a_q\right)\end{aligned} \quad (28)$$

$$\begin{aligned}&a_q\left[-jk_{\rho_m}^{TM^2}J_{\bar{n}}\left(k_{\rho_m}^{TM}a_q\right)+\vartheta kk_{\rho_m}^{TM}J_{\bar{n}}'\left(k_{\rho_m}^{TM}a_q\right)\right]\\ &\times\sum_{l=1,l\neq q}^{N_{post}}\sum_{n=-\infty}^{+\infty}A_{mnl}^{TM}H_{n-\bar{n}}^{(2)}\left(k_{\rho_m}^{TM}\left|\boldsymbol{\rho}_q-\boldsymbol{\rho}_l\right|\right)e^{-j(n-\bar{n})\phi_{lq}}\\ &+A_{m\bar{n}q}^{TM}a_q\left[-jk_{\rho_m}^{TM^2}H_{\bar{n}}^{(2)}\left(k_{\rho_m}^{TM}a_q\right)+\vartheta kk_{\rho_m}^{TM}H_{\bar{n}}^{(2)\prime}\left(k_{\rho_m}^{TM}a_q\right)\right]\\ &+\vartheta j\bar{n}k_{z_m}^{TE}J_{\bar{n}}\left(k_{\rho_m}^{TE}a_q\right)\sum_{l=1,l\neq q}^{N_{post}}\sum_{n=-\infty}^{+\infty}A_{mnl}^{TE}H_{n-\bar{n}}^{(2)}\left(k_{\rho_m}^{TE}\left|\boldsymbol{\rho}_q-\boldsymbol{\rho}_l\right|\right)e^{-j(n-\bar{n})\phi_{lq}}\\ &+\vartheta j\bar{n}A_{\bar{m}_1\bar{n}q}^{TE}k_{z_{\bar{m}_1}}^{TE}H_{\bar{n}}^{(2)}\left(k_{\rho_{\bar{m}_1}}^{TE}a_q\right)\\ &=v_{\bar{m}_1,-\bar{n}}^{TM}a_q\left[-\vartheta kk_{\rho_{\bar{m}_1}}^{TM}J_{\bar{n}}'\left(k_{\rho_{\bar{m}}}^{TM}a_q\right)+jk_{\rho_{\bar{m}_1}}^{TM^2}J_{\bar{n}}\left(k_{\rho_{\bar{m}_1}}^{TM}a_q\right)\right]\\ &-\vartheta j\bar{n}v_{\bar{m}_1,-\bar{n}}^{TE}k_{z_{\bar{m}_1}}^{TE}J_{\bar{n}}\left(k_{\rho_{\bar{m}_1}}^{TE}a_q\right)\end{aligned} \quad (29)$$

where $\vartheta = Z_s/\zeta$, and $\zeta = \sqrt{\mu_0\mu_r/\varepsilon_0\varepsilon_r}$.

Eqs.(28)-(29) are valid also for PEC posts ($Z_S = \vartheta = 0$). In this particular situation, (28)-(29) reduce to

$$J'_{\bar{n}}\left(k^{TE}_{\rho_m}a_q\right)\sum_{l=1,l\neq q}^{N_{post}}\sum_{n=-\infty}^{+\infty}A^{TE}_{mnl}H^{(2)}_{n-\bar{n}}\left(k^{TE}_{\rho_m}\left|\boldsymbol{\rho}_q-\boldsymbol{\rho}_l\right|\right)e^{-j(n-\bar{n})\phi_{lq}} + A^{TE}_{m\bar{n}q}H^{(2)\prime}_{\bar{n}}\left(k^{TE}_{\rho_m}a_q\right) = -v^{TE}_{m,-\bar{n}}J'_{\bar{n}}\left(k^{TE}_{\rho_m}a_q\right) \tag{30}$$

$$J_{\bar{n}}\left(k^{TM}_{\rho_m}a_q\right)\sum_{l=1,l\neq q}^{N_{post}}\sum_{n=-\infty}^{+\infty}A^{TM}_{mnl}H^{(2)}_{n-\bar{n}}\left(k^{TM}_{\rho_m}\left|\boldsymbol{\rho}_q-\boldsymbol{\rho}_l\right|\right)e^{-j(n-\bar{n})\phi_{lq}} + A^{TM}_{m\bar{n}q}H^{(2)}_{\bar{n}}\left(k^{TM}_{\rho_m}a_q\right) = -v^{TM}_{\bar{m}_1,-\bar{n}}J_{\bar{n}}\left(k^{TM}_{\rho_{\bar{m}_1}}a_q\right) \tag{31}$$

B. Penetrable posts

The field scattered by a penetrable (possibly lossy) post, whose radius is a_q and complex dielectric and magnetic constants are $\varepsilon_r^{(q)}, \mu_r^{(q)}$, have to grant the continuity of the total tangential electric and magnetic fields. These latter conditions, together with (27), lead to the following equations

$$\begin{aligned}
&\left[\frac{\mu_r^{(q)}k^{TE}_{\rho_{\bar{m}_2}}J_{\bar{n}}\left(k^{TE}_{\rho_{\bar{m}_2}}a_q\right)J'_{\bar{n}}\left(k^{TE(q)}_{\rho_{\bar{m}_2}}a_q\right)}{\mu_r k^{TE(q)}_{\rho_{\bar{m}_2}}H^{(2)\prime}_{\bar{n}}\left(k^{TE}_{\rho_{\bar{m}_2}}a_q\right)J_{\bar{n}}\left(k^{TE(q)}_{\rho_{\bar{m}_2}}a_q\right)} - \frac{J'_{\bar{n}}\left(k^{TE}_{\rho_{\bar{m}_2}}a_q\right)}{H^{(2)\prime}_{\bar{n}}\left(k^{TE}_{\rho_{\bar{m}_2}}a_q\right)}\right]\\
&\times\sum_{l=1,l\neq q}^{N_{post}}\sum_{n=-\infty}^{+\infty}A^{TE}_{\bar{m}_2nl}H^{(2)}_{n-\bar{n}}\left(k^{TE}_{\rho_{\bar{m}_2}}\left|\boldsymbol{\rho}_q-\boldsymbol{\rho}_l\right|\right)e^{-j(n-\bar{n})\phi_{lq}}\\
&+A^{TE}_{\bar{m}_2\bar{n}q}\left[\frac{\mu_r^{(q)}k^{TE}_{\rho_{\bar{m}_2}}H^{(2)}_{\bar{n}}\left(k^{TE}_{\rho_{\bar{m}_2}}a_q\right)J'_{\bar{n}}\left(k^{(q)TE}_{\rho_{\bar{m}_2}}a_q\right)}{\mu_r k^{TE(q)}_{\rho_{\bar{m}_2}}H^{(2)\prime}_{\bar{n}}\left(k^{TE}_{\rho_{\bar{m}_2}}a_q\right)J_{\bar{n}}\left(k^{TE(q)}_{\rho_{\bar{m}_2}}a_q\right)}-1\right]\\
&+\frac{j\bar{n}}{ka_q}\frac{k^{TM^2}_{\rho_{\bar{m}_1}}k^{TM(q)}_{z_{\bar{m}_1}}}{k^{TM(q)^2}_{\rho_{\bar{m}_1}}k^{TE}_{\rho_{\bar{m}_1}}}\left[\frac{k^{TM}_{z_{\bar{m}_1}}}{k^{TM(q)}_{z_{\bar{m}_1}}}\frac{k^{TM(q)^2}_{\rho_{\bar{m}_1}}}{k^{TM^2}_{\rho_{\bar{m}_1}}}-1\right]\frac{J_{\bar{n}}\left(k^{TM}_{\rho_{\bar{m}_1}}a_q\right)}{H^{(2)\prime}_{\bar{n}}\left(k^{TE}_{\rho_{\bar{m}_2}}a_q\right)}\\
&\times\sum_{l=1,l\neq q}^{N_{post}}\sum_{n=-\infty}^{+\infty}A^{TM}_{\bar{m}_1nl}H^{(2)}_{n-\bar{n}}\left(k^{TM}_{\rho_{\bar{m}}}\left|\boldsymbol{\rho}_q-\boldsymbol{\rho}_l\right|\right)e^{-j(n-\bar{n})\phi_{lq}}\\
&+A^{TM}_{\bar{m}_1\bar{n}q}\frac{j\bar{n}}{ka_q}\frac{H^{(2)}_{\bar{n}}\left(k^{TM}_{\rho_{\bar{m}_1}}a_q\right)k^{TM^2}_{\rho_{\bar{m}_1}}k^{TM(q)}_{z_{\bar{m}_1}}}{H^{(2)\prime}_{\bar{n}}\left(k^{TE}_{\rho_{\bar{m}_1}}a_q\right)k^{TM(q)^2}_{\rho_{\bar{m}_1}}k^{TE}_{\rho_{\bar{m}_2}}}\left[\frac{k^{TM}_{z_{\bar{m}_1}}k^{TM(q)^2}_{\rho_{\bar{m}_1}}}{k^{TM(q)}_{z_{\bar{m}_1}}k^{TM^2}_{\rho_{\bar{m}_1}}}-1\right]\\
&=-v^{TE}_{\bar{m}_2,-\bar{n}}\left[\frac{\mu_r^{(q)}k^{TE}_{\rho_{\bar{m}_2}}J_{\bar{n}}\left(k^{TE}_{\rho_{\bar{m}_2}}a_q\right)J'_{\bar{n}}\left(k^{TE(q)}_{\rho_{\bar{m}_2}}a_q\right)}{\mu_r k^{TE(q)}_{\rho_{\bar{m}_2}}H^{(2)\prime}_{\bar{n}}\left(k^{TE}_{\rho_{\bar{m}_2}}a_q\right)J_{\bar{n}}\left(k^{TE(q)}_{\rho_{\bar{m}_2}}a_q\right)} - \frac{J'_{\bar{n}}\left(k^{TE}_{\rho_{\bar{m}_2}}a_q\right)}{H^{(2)\prime}_{\bar{n}}\left(k^{TE}_{\rho_{\bar{m}_2}}a_q\right)}\right]\\
&-v^{TM}_{\bar{m},-\bar{n}}\frac{j\bar{n}}{ka_q}\frac{k^{TM^2}_{\rho_{\bar{m}_1}}k^{TM(q)}_{z_{\bar{m}_1}}}{k^{TM(q)^2}_{\rho_{\bar{m}_1}}k^{TE}_{\rho_{\bar{m}_1}}}\left[\frac{k^{TM}_{z_{\bar{m}_1}}k^{TM(q)^2}_{\rho_{\bar{m}_1}}}{k^{TM(q)}_{z_{\bar{m}_1}}k^{TM^2}_{\rho_{\bar{m}_1}}}-1\right]\frac{J_{\bar{n}}\left(k^{TM}_{\rho_{\bar{m}_1}}a_q\right)}{H^{(2)\prime}_{\bar{n}}\left(k^{TE}_{\rho_{\bar{m}_1}}a_q\right)}
\end{aligned} \tag{32}$$

$$\begin{aligned}
&\left[\frac{J'_{\bar{n}}\left(k^{TM}_{\rho_{\bar{m}_1}}a_q\right)}{H^{(2)\prime}_{\bar{n}}\left(k^{TM}_{\rho_{\bar{m}_1}}a_q\right)} - \frac{\varepsilon_r^{(q)}k^{TM}_{\rho_{\bar{m}_1}}J_{\bar{n}}\left(k^{TM}_{\rho_{\bar{m}_1}}a_q\right)J'_{\bar{n}}\left(k^{TM(q)}_{\rho_{\bar{m}_1}}a_q\right)}{\varepsilon_r k^{TM(q)}_{\rho_{\bar{m}_1}}H^{(2)\prime}_{\bar{n}}\left(k^{TM}_{\rho_{\bar{m}_1}}a_q\right)J_{\bar{n}}\left(k^{TM(q)}_{\rho_{\bar{m}_1}}a_q\right)}\right]\\
&\times\sum_{l=1,l\neq q}^{N_{post}}\sum_{n=-\infty}^{+\infty}A^{TM}_{\bar{m}nl}H^{(2)}_{n-\bar{n}}\left(k^{TM}_{\rho_{\bar{m}_1}}\left|\boldsymbol{\rho}_q-\boldsymbol{\rho}_l\right|\right)e^{-j(n-\bar{n})\phi_{lq}}\\
&+A^{TM}_{\bar{m}_1\bar{n}q}\left[1-\frac{\varepsilon_r^{(q)}k^{TM}_{\rho_{\bar{m}_1}}H^{(2)}_{\bar{n}}\left(k^{TM}_{\rho_{\bar{m}_1}}a_q\right)J'_{\bar{n}}\left(k^{TM(q)}_{\rho_{\bar{m}_1}}a_q\right)}{\varepsilon_r k^{TM(q)}_{\rho_{\bar{m}_1}}H^{(2)\prime}_{\bar{n}}\left(k^{TM}_{\rho_{\bar{m}_1}}a_q\right)J_{\bar{n}}\left(k^{TM(q)}_{\rho_{\bar{m}_1}}a_q\right)}\right]\\
&+\frac{j\bar{n}}{ka_q}\frac{k^{TE}_{z_{\bar{m}_2}}}{k^{TM}_{\rho_{\bar{m}_1}}}\left[1-\frac{k^{TE^2}_{\rho_{\bar{m}_2}}k^{TE(q)}_{z_{\bar{m}_1}}}{k^{TE(q)^2}_{\rho_{\bar{m}_2}}k^{TE}_{z_{\bar{m}_2}}}\right]\frac{J_{\bar{n}}\left(k^{TE}_{\rho_{\bar{m}_2}}a_q\right)}{H^{(2)\prime}_{\bar{n}}\left(k^{TM}_{\rho_{\bar{m}_1}}a_q\right)}\\
&\times\sum_{l=1,l\neq q}^{N_{post}}\sum_{n=-\infty}^{+\infty}A^{TE}_{\bar{m}_2nl}H^{(2)}_{n-\bar{n}}\left(k^{TE}_{\rho_{\bar{m}_2}}\left|\boldsymbol{\rho}_q-\boldsymbol{\rho}_l\right|\right)e^{-j(n-\bar{n})\phi_{lq}}\\
&+A^{TE}_{\bar{m}_1\bar{n}q}\frac{j\bar{n}}{ka_q}\frac{k^{TE}_{z_{\bar{m}_2}}}{k^{TM}_{\rho_{\bar{m}_1}}}\left[1-\frac{k^{TE^2}_{\rho_{\bar{m}_2}}k^{TE(q)}_{z_{\bar{m}_2}}}{k^{TE(q)^2}_{\rho_{\bar{m}_2}}k^{TE}_{z_{\bar{m}_2}}}\right]\frac{H^{(2)}_{\bar{n}}\left(k^{TE}_{\rho_{\bar{m}_2}}a_q\right)}{H^{(2)\prime}_{\bar{n}}\left(k^{TM}_{\rho_{\bar{m}_1}}a_q\right)}\\
&=-v^{TM}_{\bar{m}_1,-\bar{n}}\left[\frac{J'_{\bar{n}}\left(k^{TM}_{\rho_{\bar{m}_1}}a_q\right)}{H^{(2)\prime}_{\bar{n}}\left(k^{TM}_{\rho_{\bar{m}_1}}a_q\right)} - \frac{\varepsilon_r^{(q)}k^{TM}_{\rho_{\bar{m}_1}}J_{\bar{n}}\left(k^{TM}_{\rho_{\bar{m}_1}}a_q\right)J'_{\bar{n}}\left(k^{TM(q)}_{\rho_{\bar{m}_1}}a_q\right)}{\varepsilon_r k^{TM(q)}_{\rho_{\bar{m}_1}}H^{(2)\prime}_{\bar{n}}\left(k^{TM}_{\rho_{\bar{m}_1}}a_q\right)J_{\bar{n}}\left(k^{TM(q)}_{\rho_{\bar{m}_1}}a_q\right)}\right]\\
&-v^{TE}_{\bar{m},-\bar{n}}\frac{j\bar{n}}{ka_q}\frac{k^{TE}_{z_{\bar{m}_2}}}{k^{TM}_{\rho_{\bar{m}_1}}}\left[1-\frac{k^{TE^2}_{\rho_{\bar{m}_2}}k^{TE(q)}_{z_{\bar{m}_1}}}{k^{TE(q)^2}_{\rho_{\bar{m}_2}}k^{TE}_{z_{\bar{m}_2}}}\right]\frac{J_{\bar{n}}\left(k^{TE}_{\rho_{\bar{m}_2}}a_q\right)}{H^{(2)\prime}_{\bar{n}}\left(k^{TM}_{\rho_{\bar{m}_1}}a_q\right)}
\end{aligned} \tag{33}$$

C. Determination of the expansion coefficients

Let the structure under analysis be composed by N posts. In order to numerically solve the equations (28)-(32), the number of retained azimuthally and vertical modes N_ϕ and N_z, respectively, can be chosen according to [21],[23].

Since vertical modes with different orders *m* are decoupled, it is possible to cast (28)-(32) for each value $m = 1,\ldots,N_z$ into the following matrix form

$$\begin{bmatrix}\underline{\mathbf{T}}^{TM,TM}_m & \underline{\mathbf{T}}^{TM,TE}_m\\ \underline{\mathbf{T}}^{TE,TM}_m & \underline{\mathbf{T}}^{TE,TE}_m\end{bmatrix}\begin{bmatrix}\mathbf{A}^{TM}_m\\ \mathbf{A}^{TE}_m\end{bmatrix} = \boldsymbol{\Omega}^{TM+TE}_m \tag{34}$$

where $\underline{\mathbf{T}}_m$ are the post interaction coupling matrices, $\left[\mathbf{A}^{TM}_m, \mathbf{A}^{TE}_m\right]^T$ is the unknown vector containing all the cylindrical waves coefficients and $\boldsymbol{\Omega}^{TM/TE}_m$ is the excitation vector. The unknown field coefficients are then found by solving a N_z matrix equations (33).

V. Input Parameters

In this Section we discuss the definition of excitation ports and the calculation of the input parameters, starting from the results obtained from the procedure described in the previous sections. Source modeling for specific geometries have been proposed in the past as in [21][34]. Here we follow the

formulation in [21]. We only outline the differences with the PEC walls case for a waveguide port excitation and a general excitation defined over the impedance walls (coaxial excitation, slots).

A. Waveguide Ports: Computation of the Input Parameters

The computation of the input parameters is performed according to the same approach presented in [21]. Once the *j*-th input port is fed with the equivalent magnetic current $\mathbf{h}_j$, a modal decomposition is performed on the total magnetic field $\mathbf{H}_i$ at the *i*-th port for each *i*, by projecting $\mathbf{H}_i$ on the rectangular waveguide modes $\mathbf{h}_{nm}$ (the TE_{10} fundamental mode is used in the following, being usually sufficient for our scopes). The field $\mathbf{H}_i$ can be decomposed in a field $\underline{\mathbf{G}}^{\mathrm{PPW}}\left(\mathbf{r}_q,\mathbf{r}_j\right)\cdot\mathbf{h}_j^{\mathrm{TE}_{01}}\left(\mathbf{r}_j\right)$ excited in the absence of posts (i.e., computed through the PPW Green's function) and a field $\mathbf{H}^{\mathrm{Posts}}$ scattered by posts (determined through the mode matching)

$$\begin{aligned} Y_{qj} &= j\omega\varepsilon Z_w^q Z_w^j \\ &\cdot\int_{P_q}\int_{P_j}\mathbf{h}_q^{\mathrm{TE}_{01}}\left(\mathbf{r}_q\right)\cdot\underline{\mathbf{G}}^{\mathrm{PPW}}\left(\mathbf{r}_q,\mathbf{r}_j\right)\cdot\mathbf{h}_j^{\mathrm{TE}_{01}}\left(\mathbf{r}_j\right)dS_j dS_q \\ &+ Z_w^{P_q}\int_{P_q}\mathbf{h}_q^{\mathrm{TE}_{01}}\left(\mathbf{r}_q\right)\cdot\mathbf{H}^{\mathrm{Posts}}\left(\mathbf{r}_q\right)dS_q = Y^{\mathrm{PPW}}+Y^{\mathrm{Posts}} \end{aligned} \quad (35)$$

The computation of Y^{PPW} can be performed by moving on the current $\mathbf{h}$ the derivatives present in the definition of the Green's function. The details are shown in [21], while an efficient computation of Y^{Posts} has been presented in [23].

However, the presence of impedance boundary condition on the PPW plates leads to a different integral expression for Y^{PPW}. In fact in this new structure, since the TM and TE radial wavenumbers are different, the *z*-derivative of the scalar potential S^{TE} does not cancel out the scalar potential S^{TM}. Following [24], after a lengthy calculation, the final expression for Y^{PPW} is

$$\begin{aligned} Y_{qj}^{PPW} &= -\frac{Z_w^q Z_w^j}{j\omega\mu}\int_{P_q}\int_{P_j}\partial_u h_q^{\mathrm{TE}_{01}}\partial_{u'}h_j^{\mathrm{TE}_{01}}\left[-k^2 S^{\mathrm{TM}}\left(\mathbf{r},\mathbf{r}'\right)\right. \\ &\left. + k^2 S^{\mathrm{TE}}\left(\mathbf{r},\mathbf{r}'\right) - \tilde{G}^{\mathrm{TE}}\left(\mathbf{r},\mathbf{r}'\right)\right]dS'dS \\ &-\frac{Z_w^q Z_w^j}{j\omega\mu}k^2\left(\hat{\mathbf{u}}_q\cdot\hat{\mathbf{u}}_j\right)\int_{P_q}\int_{P_j}h_q^{\mathrm{TE}_{01}}\left(\mathbf{r}_q\right)G^{\mathrm{TM}}\left(\mathbf{r},\mathbf{r}'\right)h_j^{\mathrm{TE}_{01}}\left(\mathbf{r}_j\right)dS'dS \end{aligned} \quad (36)$$

where $\tilde{G}^{\mathrm{TE}}$ is a dual TE Green's function (appearing in [24] in connection with slot modeling). It corresponds to the current in a TE equivalent transmission line fed by a unit series voltage generator, as opposed to the conventional G^{TE} Green's function (a voltage in a TE equivalent transmission line fed by a unit shunt current generator) [28].

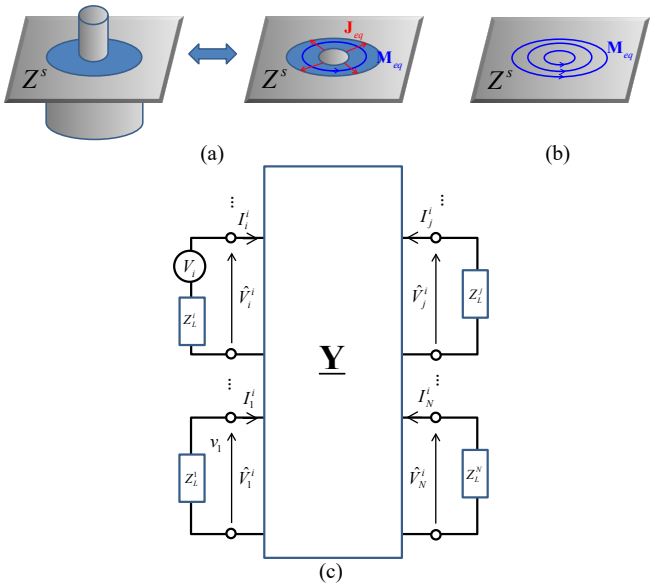

Fig. 4. (a) Coaxial excitation's equivalent electric and magnetic currents. (b) Magnetic sources defined over the impedance condition used in the mode-matching technique. (c) Equivalent Y model of the SIW device under analysis.

B. Coaxial Cables and slots: Computation of the Admittance Matrix

Coaxial cables can be described through equivalent currents placed on one of the PPW plates [21], as shown in Fig. 4a. However, due to the presence of losses, the equivalent input and output magnetic currents are not placed on PEC plates (i.e., short circuits), as required by the definition of the admittance matrix. In order to keep the formulation simpler and similar to that one of PEC case, only the magnetic currents defined over the uniform impedance wall are used as source (Fig. 4b). In a SIW system excited by *N* coaxial ports (with inner radius a_j and outer radius b_j), this particular feeding choice leads to the equivalent network illustrated in Fig. 4c, where further impedances

$$Z_L^j = \frac{1}{2\pi}\ln\left(\frac{b_j}{a_j}\right)\sqrt{\frac{\mu}{\varepsilon}} = \frac{1}{2\pi}\ln\left(\frac{b_j}{a_j}\right)\sqrt{\frac{\omega\mu}{\sigma}}\frac{1}{\sqrt{2}}(1+j) \quad (37)$$

are connected to the input ports.

For this reason, once the output currents at each port are determined for each feeding configuration, we need to perform a post processing ready to compute the correct admittance matrix $\underline{\mathbf{Y}}$ of the structure.

Let us feed the *i*-th port with a voltage V_i, as shown in Fig. 4c. The procedure proposed in [21] allows computing the output current on the *j*-th port I_j^i. The ratio I_j^i/V_i is the *ij* element of the matrix $\underline{\mathbf{Y}}_L$. On the other hand, the entries of the admittance matrix $\underline{\mathbf{Y}}$ are defined with respect to the voltages $\hat{V}_i^i$ at the input of the *N*-port network, i.e., *after* each impedance Z_L.

We can write

$$\hat{\mathbf{V}}_i = -\underline{\mathbf{Z}}_L \mathbf{I}_i + \mathbf{V}_i \tag{38}$$

where we have defined the column vectors

$$\hat{\mathbf{V}}_i = \begin{pmatrix} \hat{V}_1^i \\ \vdots \\ \hat{V}_i^i \\ \vdots \\ \hat{V}_N^i \end{pmatrix}, \qquad \mathbf{I}_i = \begin{pmatrix} I_1^i \\ \vdots \\ I_i^i \\ \vdots \\ I_N^i \end{pmatrix}, \qquad \mathbf{V}_i = \begin{pmatrix} 0 \\ \vdots \\ V_i \\ \vdots \\ 0 \end{pmatrix} \tag{39}$$

and the diagonal matrix

$$\underline{\mathbf{Z}}_L = \begin{bmatrix} Z_L^1 & \dots & 0 \\ & & \\ 0 & \dots & Z_L^N \end{bmatrix}. \tag{40}$$

Since for every i

$$\mathbf{I}_i = \underline{\mathbf{Y}} \cdot \hat{\mathbf{V}}_i \tag{41}$$

we can replace (38) into (41)

$$\mathbf{I}_i = -\underline{\mathbf{Z}}_L \underline{\mathbf{Y}} \cdot \mathbf{I}_i + \underline{\mathbf{Y}} \cdot \mathbf{V}_i \tag{42}$$

Once N different simulations are performed, one for each excitation, we can define the following matrices

$$\underline{\mathbf{I}} = \left(\mathbf{I}_1 \quad \cdots \quad \mathbf{I}_N\right), \qquad \underline{\mathbf{V}} = \left(\mathbf{V}_1 \quad \cdots \quad \mathbf{V}_N\right) \tag{43}$$

and the following relation holds

$$\underline{\mathbf{I}} = \underline{\mathbf{Y}} \cdot \left(\underline{\mathbf{V}} - \underline{\mathbf{Z}}_L \underline{\mathbf{I}}\right) \quad \Rightarrow \quad \underline{\mathbf{Y}} = \underline{\mathbf{I}} \cdot \left(\underline{\mathbf{V}} - \underline{\mathbf{Z}}_L \underline{\mathbf{I}}\right)^{-1} \tag{44}$$

By replacing in (44) the simulated results $\mathbf{I} = \underline{\mathbf{Y}}_L \cdot \underline{\mathbf{V}}$, we finally obtain a simple expression for the admittance matrix $\underline{\mathbf{Y}}$

$$\underline{\mathbf{Y}} = \underline{\mathbf{Y}}_L \cdot \underline{\mathbf{V}} \cdot \left(\underline{\mathbf{V}} - \underline{\mathbf{Z}}_L \cdot \underline{\mathbf{V}}\right)^{-1} \tag{45}$$

If the same excitation is assumed for all the ports, $\underline{\mathbf{V}} = V \underline{\mathbf{1}}$ ($\underline{\mathbf{1}}$ being the identity matrix) and

$$\underline{\mathbf{Y}} = \underline{\mathbf{Y}}_L \cdot \left(\underline{\mathbf{1}} - \underline{\mathbf{Z}}_L \underline{\mathbf{Y}}_L\right)^{-1} \tag{46}$$

An equivalent of the above mentioned procedure could be obtained in terms of equivalent currents, by using the results in [24]. A slot excitation can be described only with equivalent magnetic currents allowing the use of the procedure presented in [23] to study multi-waveguide SIW systems.

VI. Numerical Results

In this section we apply the rigorous and approximated proposed methods for the analysis of SIW microwave devices available in the scientific literature. Four examples have been selected in order to test different features of the method. All the results have been compared with numerical simulation performed with the finite elements commercial software Ansys HFSS™ 15. For the reader's convenience the measured parameters taken from the original articles are also included.

The first example is a frequency-selective power combiner/divider [35]. The structure and the relevant geometrical parameters are given in Fig. 5. The structure is composed by 108 copper posts and is fed by four waveguide ports, each one modeled through an array of PEC posts [21]. The *S*-parameters of the structures computed with the rigorous and approximated methods are compared to HFSS™ simulations in Fig. 6. A very good agreement is found among all these methods and the measurements performed in [21].

The second example is the SIW right-angle corner proposed in [36]. It consists of 32 copper posts in a corner arrangement and 273 air posts working as an integrated lens. The transition is fed by 2 ports. The top view of the structure is shown in Fig. 7. The interest of this test case is the presence of a large number of dielectric posts. Fig. 8 compares the calculated scattering parameters. A very good agreement is obtained between the simulated transmission parameters S_{12}. Small differences in the reflection parameter S_{11} are due to the very low level of this parameter.

The third example is a linear phase filter [37] composed by 80 copper posts and 4 rectangular slots acting as reactive loads. The complete structure is shown in

Fig. 9. The slots are modeled according to the method of moments approach described in [24] by using 5 entire domain basis functions for each slot. The slots admittances are modified according to Section V to rigorously take into account losses. The relevant results are plotted in Fig. 10.

The last example is a large system implementing a generalized Chebychev diplexer [38], composed by 414 copper posts and fed by 3 ports shown in Fig. 11. Also for this last case (see Fig. 12), a very good agreement between scattering parameters is obtained.

We report in Tables I and II the CPU time and used memory for the considered cases and compare them to those of HFSS™. The data have been generated using a Personal Computer with a 2.8 GHz Intel I7 870 CPU, while the proposed methods have been implemented in Matlab™. The actual implementation of the codes does not take advantage of multi-core or multi-CPU systems, but it can be parallelized.

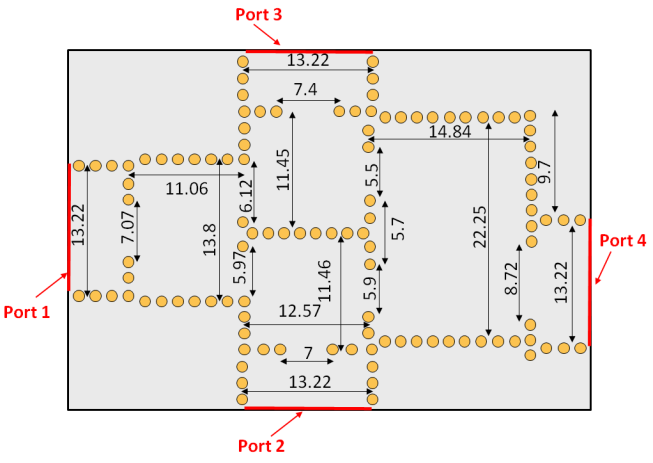

Fig. 5. Geometry of the frequency-selective power combiner/divider [35]. Physical parameters of the substrate: height h = 0.508 mm, relative permittivity ε_r=2.33, loss tangent $\tan\delta$ = 0.0012. All dimensions are expressed in millimeters.

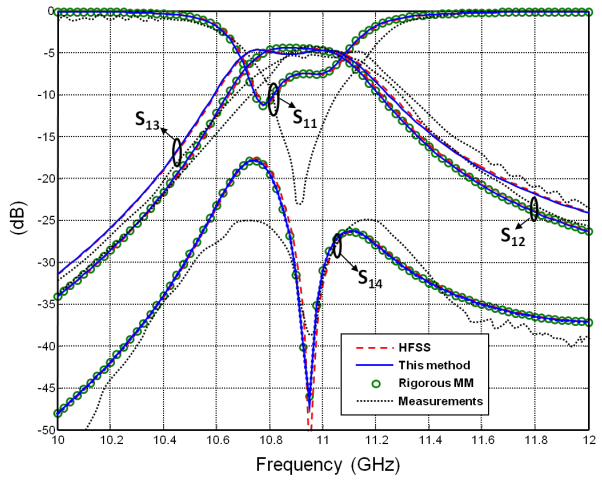

(a)

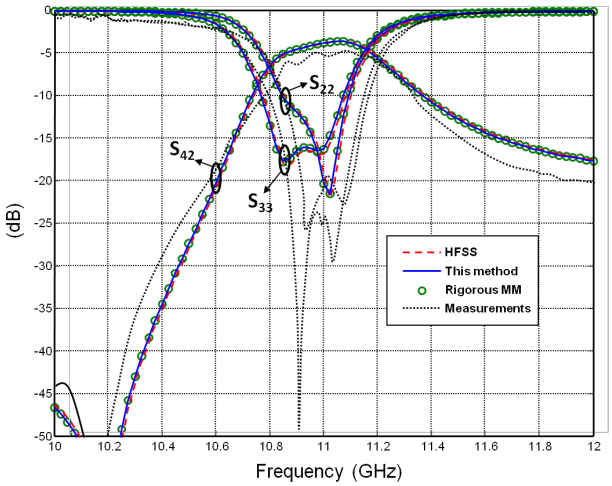

(b)

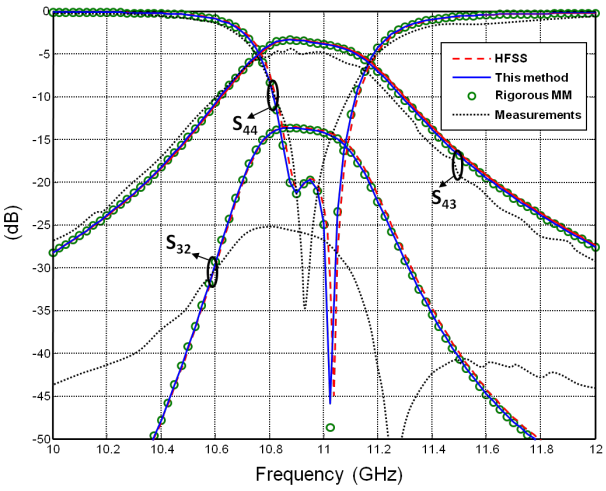

(c)

Fig. 6. Comparison of the magnitude of the scattering parameters for the test structure represented in Fig. 5: this method (*blue solid lines*), rigorous method (*green circles*), HFSS^{TM} (*red dashed lines*) and measurements (*black dotted lines*). (a) S_{1X} parameters, (b) S_{2X} parameters, (c) S_{3X} parameters. Measurements taken from [21].

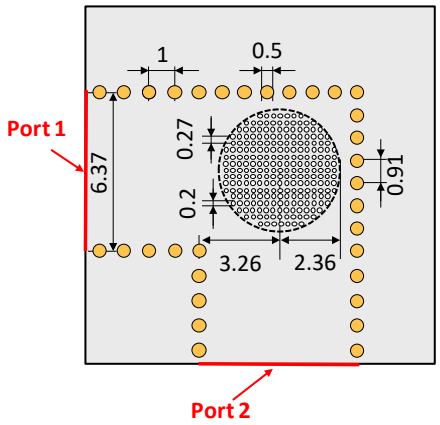

Fig. 7. SIW right-angle corner [36]. Physical parameters of the substrate: height h = 0.508 mm, relative permittivity ε_r = 4.5, loss tangent tanδ = 0.002. All dimensions are expressed in millimeters.

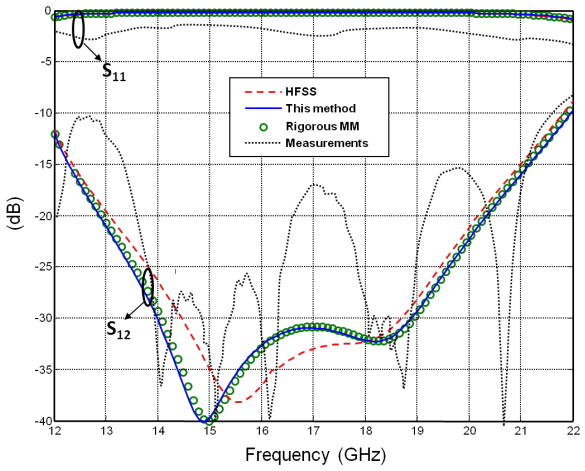

Fig. 8. Comparison of the magnitude of the scattering parameters for the structure represented in Fig. 7: this method (*blue solid lines*), rigorous method (*green circles*), HFSS^{TM} (*red dashed lines*) and measurements (*black dotted lines*). Measurements taken from [36].

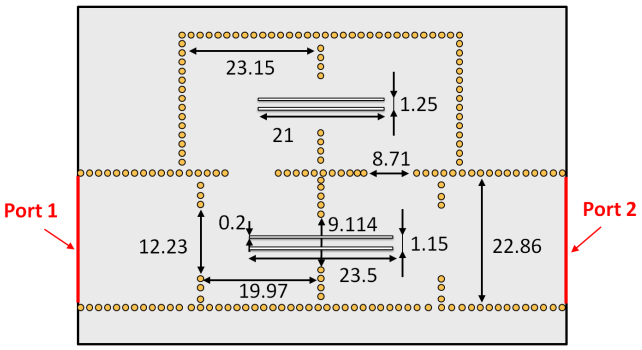

Fig. 9. Geometry of the linear phase filter in quadruplet topology with frequency-dependent couplings [37]. Physical parameters of the substrate: height h=0.762, relative permittivity ε_r=3.46, loss tangent tanδ=0.0018. All dimensions are expressed in millimeters.

These results demonstrate that the proposed algorithm is extremely efficient both in terms of computational and memory requirements. Moreover, since it does not need any meshing, it can play a key-role in design optimization procedures where geometrical parameters are changed.

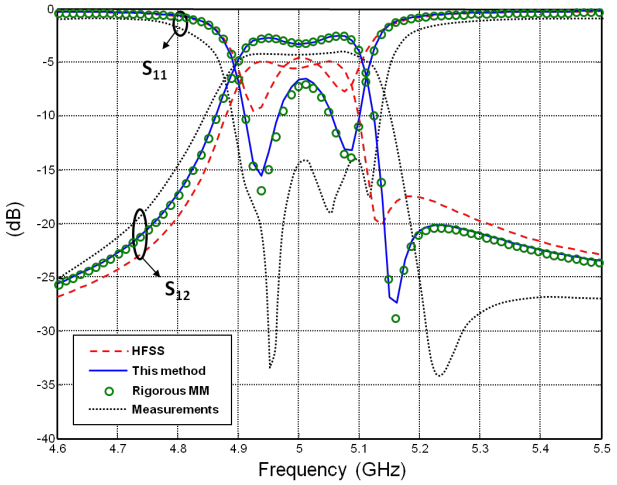

Fig. 10. Comparison of the magnitude of the scattering parameters for the structure represented in Fig. 9: this method (*blue solid lines*), rigorous method (*green circles*), HFSS™ (*red dashed lines*) and measurements (*black dotted lines*). Measurements taken from [37].

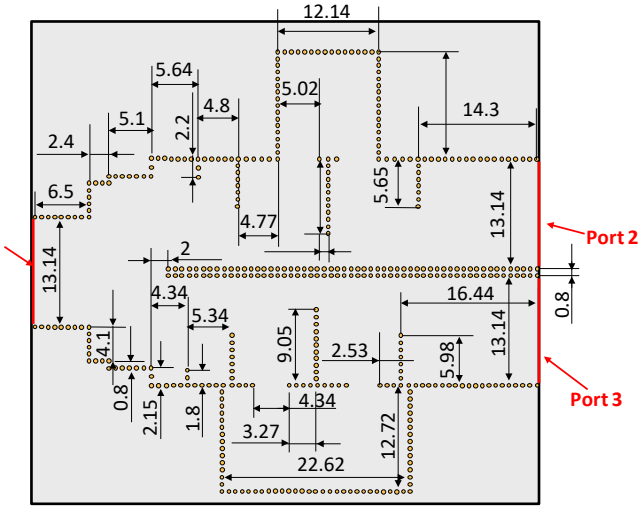

Fig. 11. Geometry of the generalized Chebyshev SIW diplexer [38]. Physical parameters of the substrate: height h= 0.762 mm, relative permittivity ε_r=3.46, loss tangent tanδ = 0.0018. All dimensions are expressed in millimeters.

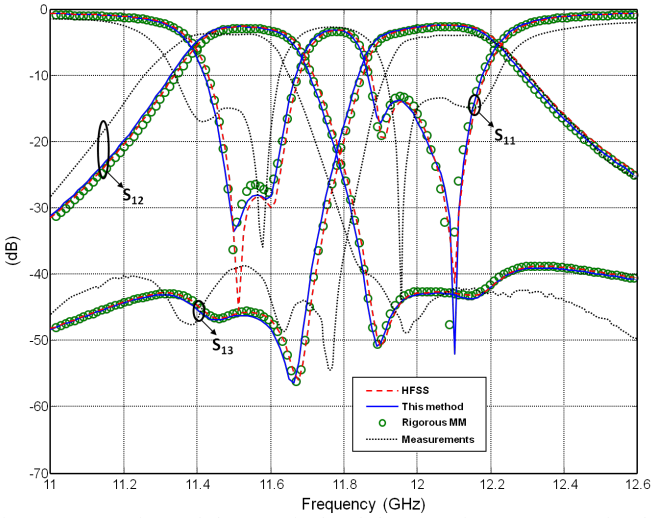

Fig. 12. Comparison of the magnitude of the scattering parameters for the structure represented in Fig. 11. This method (*blue solid lines*), rigorous method (*green circles*), HFSS™ (*red dashed lines*) and measurements (*black dotted lines*). Measurements taken from [38].

TABLE I

CPU SIMULATION TIME ON A XEON E5540 2.83 GHZ WITH 16 GBYTE RAM

Structure	Metallic / dielectric posts	HFSS		This paper
		Mesh	Freq. Point	
Power combiner	108 / 0	99 s	7 s	1.58 s
Matched corner	32 / 273	2012 s	585 s	9.04 s
Linear ph. Filter	80 / 0	585 s	137 s	9.76 s
Cheb. diplexer	414 / 0	746 s	35 s	10.2 s

TABLE II

MEMORY USED ON A XEON E5540 2.83 GHZ WITH 16 GBYTE RAM

Structure	Metallic/dielect posts	HFSS		This paper
		Mesh	Freq. Point	
Power combiner	108 / 0	254 MB	252 MB	60 MB
Matched corner	32 / 273	4.55 GB	4.55 GB	200 MB
Linear ph. shifter	80 / 0	1.72 GB	1.71 GB	90 MB
Cheb. diplexer	414 / 0	1.02 GB	1.02 GB	320 MB

VII. CONCLUSION

We have presented here a rigorous approach for the full-wave analysis of lossy SIW devices. A modified boundary Green's function taking into account the losses on the waveguide plates is used. Different kinds of boundary conditions are imposed on the later surface of the posts, according to their nature: good conducting posts are described through a Leontovich condition, while field continuity is imposed on the surface of dielectric posts, possibly lossy. A rigorous calculation of the input parameters is also given, for different kind of excitations. At microwaves regime, an approximated formulation based on the physical properties of these devices has been introduced. Numerical results relevant to real microwave devices making use of metallic and dielectric posts have been presented and validated by full-wave simulations with commercial software (HFSS™). An excellent agreement is obtained for all cases with reduced computational time and memory occupation, making this method suitable to be used in optimization procedures.

APPENDIX

In the following the superscripts $^{(1)}$ and $^{(2)}$ refer to media with parameters $\varepsilon_r^{(1)}, \mu_r^{(1)}$ and $\varepsilon_r^{(2)}, \mu_r^{(2)}$, respectively.

The amplitudes $\Delta_{m,n}$ in (27) depend on physical and geometrical parameters as follow:

$$\Delta_{m,m}^{TE,TE} = \frac{1}{\omega h\left(\mu^{(1)}-\mu^{(2)}\right)}\left(\frac{\mu^{(2)}}{\mu^{(1)}}-\frac{\mu^{(1)}}{\mu^{(2)}}\right)$$

$$\Delta_{m,n}^{TM,TE'} = \begin{cases} \dfrac{-6\omega\varepsilon^{(1)}h+\dfrac{2m^2\pi^2}{\omega h\mu^{(2)}}+\dfrac{4\omega^3\left(\varepsilon^{(1)}\right)^2\mu^{(2)}h^3}{m^2\pi^2}}{m^2\pi^2-\omega^2\mu^{(2)}\varepsilon^{(1)}h^2} & m=n \\ \dfrac{\left((-1)^{n+m}+1\right)}{\left(n^2-m^2\right)}\left(\dfrac{2\omega n\varepsilon^{(1)}}{\pi}-\dfrac{2nm^2\pi}{\omega h^2\mu^{(2)}}\right) & m\neq n \end{cases}$$

$$\Delta_{m,n}^{TM,TM} = \begin{cases} 2\dfrac{h\omega}{m^2\pi^2}\left(\varepsilon^{(1)}+\varepsilon^{(2)}\right) & m=n \\ 4\dfrac{\omega h}{\pi^2\left(m^2-n^2\right)}\left(\varepsilon^{(1)}-\varepsilon^{(2)}\right)\left(1+\left(-1\right)^{m+n}\right) & m\neq n \end{cases}$$

$$\Delta_{m,n}^{TE,TM'} = \begin{cases} 2\dfrac{1}{h\omega\mu^{(2)}}+\left[4\dfrac{1}{h}+2\dfrac{m^2\pi^2}{\omega^2h^3\varepsilon^{(1)}\mu^{(2)}}-4\dfrac{\omega^2\varepsilon^{(1)}\mu^{(2)}h}{m^2\pi^2}\right] \\ \times\left(\dfrac{h^2\omega\varepsilon^{(1)}}{m^2\pi^2-h^2\omega^2\varepsilon^{(1)}\mu^{(2)}}\right) & m=n \\ 2\dfrac{n\left(\left(-1\right)^{n+m}+1\right)}{\left(n^2-m^2\right)}\left[\dfrac{n^2\pi}{h^2\omega\mu_2}-\dfrac{\omega\varepsilon^{(1)}}{\pi}\right] & m\neq n \end{cases} \quad (47)$$

REFERENCES

[1] D. Deslandes and K. Wu, "Integrated microstrip and rectangular waveguide in planar form," *IEEE Microw. Wirel. Comp. Lett*., vol. 11, no. 2, pp. 68 – 70, Feb. 2001.

[2] J. Hirokawa and M. Ando, "Single-layer feed waveguide consisting of posts for plane TEM wave excitation in parallel plates," *IEEE Trans. Microw. Theory Techn.*, vol. 46, no. 5, pp. 625–630, May. 1998.

[3] F. Xu and K. Wu., "Guided-wave and leakage characteristics of substrate integrated waveguide," *IEEE Trans. Microw. Theory Techn.*, vol. 53, no. 1, pp. 66 – 73, Jan. 2005.

[4] Xiao-Ping Chen and Ke Wu, "Substrate Integrated Waveguide Filters: Design Techniques and Structure Innovations," *IEEE Microwave Magazine*, vol.15, no.6, pp.121-133, Sept.-Oct. 2014.

[5] S. Park, Y. Okajima, J. Hirokawa, and M. Ando, "A slotted post-wall waveguide array with interdigital structure for 45° linear and dual Polarization," *IEEE Trans. Antennas Propag*., vol. 53, no. 9, pp. 2865 – 2871, Sep. 2005.

[6] M. Ettorre, A. Neto, G. Gerini, and S. Maci, "Leaky-wave slot array antenna fed by a dual reflector system," *IEEE Trans. Antennas Propag.*, vol. 56, no. 10, pp. 3143 – 3149, Oct. 2008.

[7] M. Ettorre, R. Sauleau, and L. Le Coq, "Multi-beam multi-layer leakywave SIW pillbox antenna for millimetre-wave applications," *IEEE Trans. Antennas Propag*., vol. 59, no. 4, pp. 1093 – 1100, Apr. 2011.

[8] J. Xu, Z.N. Chen, X. Qing, and W. Hong, "140-GHz TE_{20}-mode dielectric-loaded SIW slot antenna array in LTCC," *IEEE Trans. Antennas Propag*., vol. 61, no. 4, pp. 1784 – 1793, Apr. 2013.

[9] H. J. Tang, W. Hong, J. Chen, G. Q. Luo, and K. Wu , "Development of millimeter-wave planar diplexers based on complementary characters of dual-mode substrate integrated waveguide filters with circular and elliptic cavities," *IEEE Trans. Microw. Theory Techn.*, vol. 55, no. 4, pp. 776 – 782, Apr. 2007.

[10] R. Moro, S. Kim, M. Bozzi and M. Tentzeris "Inkjet-printed paper-based substrate-integrated waveguide (SIW) components and antennas," *Int. J. of Microw. and Wireless Technologies*, 5, pp 197-204, 2013.

[11] F. Xu, Y. Zhang, W. Hong, K. Wu, and T. J. Cui, "Finite-difference frequency-domain algorithm for modeling guided-wave properties of substrate integrated waveguide," *IEEE Trans. Microw. Theory Techn.*, vol. 51, no. 11, pp. 2221–2227, Nov. 2003.

[12] D. Deslandes and K. Wu, "Accurate modeling, wave mechanisms, and design considerations of a substrate integrated waveguide," *IEEE Trans. Microw. Theory Tech*, vol. 54, no. 6, pp. 2516 – 2526, Jun. 2006.

[13] M. Bozzi, L. Perregrini, and K. Wu, "Modeling of conductor, dielectric, and radiation losses in substrate integrated waveguide by the boundary integral-resonant mode expansion method," *IEEE Trans. Microw. Theory Tech*, vol. 56, no. 12, pp.3153 – 3161, Dec. 2008.

[14] B. Tomasic and A. Hessel, "Linear array of coaxially fed monopole elements in a parallel plate waveguide – Part I: Theory," *IEEE Trans. Antennas Propag*., vol. 36, no. 4, pp. 449 – 462, Apr. 1988.

[15] L. Tsang, H. Chen, C. C. Huang, and V. Jandhyala, "Modeling of multiple scattering among vias in planar waveguides using Foldy–Lax equations," *Microwave Optical Technol. Lett*., vol. 31, pp. 201–208, 2001.

[16] C. C. Huang , L. Tsang, and C. H. Chan, "Multiple scattering among vias in lossy planar waveguides using SMCG method," *IEEE Trans. Adv. Pack.*, vol. 25, no. 2, pp. 181 – 188, May 2002.

[17] H. R. Sadreazami, E. Mehrshahi, and R. Rezaiesarlak, "Analysis of dispersion characteristic of substrate integrated waveguide based on mode matching method," *IEEE APEMC*, 12-16 Avr. 2010, Beijing, China.

[18] Z. Kordiboroujeni and J. Bornemann, "Mode-matching analysis and design of substrate integrated waveguide T-junction diplexer and corner filter," *Int. J. Numer. Model*., 2015.

[19] X. H. Wu and A. A. Kishk, "Hybrid of method of moments and cylindrical eigenfunction expansion to study substrate integrated waveguide circuits," *IEEE Trans. Microw. Theory Techn.*, vol. 56, no. 10, pp. 2270 – 2270, Oct. 2008.

[20] E. Arnieri, G. Amendola, "Analysis of Substrate Integrated Waveguide Structures Based on the Parallel-Plate Waveguide Green's Function," *IEEE Transactions on Microwave Theory and Techn.*, vol. 56, no. 7, pp. 1615-1623, July 2008.

[21] M. Casaletti, R. Sauleau, M. Ettorre, and S. Maci, "Efficient analysis of metallic and dielectric posts in parallel-plate waveguide structures," *IEEE Trans. Microw. Theory Techn.*, vol. 60, no. 12, pp. 2979 – 2989, Oct. 2012.

[22] M. Albani, A. Mazzinghi, and A. Freni, "Automatic design of CP-RLSA antennas," *IEEE Trans. Antennas Propag.*, vol. 60, no. 12, pp. 5538 – 5547, Dec. 2012.

[23] M. Casaletti, G. Valerio, J. Seljan, M. Ettorre, and R. Sauleau, "A full-wave hybrid method for the analysis of multilayered SIW-based antennas," *IEEE Trans. Antennas. Propag.*, vol. 61, no. 11, pp. 5575 – 5588, Nov. 2013.

[24] M. Albani, A. Mazzinghi, and A. Freni, "Rigorous MoM analysis of finite conductivity effects in RLSA antennas," *IEEE Trans. Antennas Propag*, vol. 59, no. 11, pp. 4023 – 4032, Nov. 2011.

[25] M. Casaletti, G. Valerio, R. Sauleau, and M. Albani, "Rigorous losses evaluation in the numerical analysis of SIW structures," *European Conf. Antennas Propag.* (*EuCAP 2015*), 12-17 Apr. 2015, Lisbon, Portugal.

[26] M. Casaletti, G. Valerio, J. Seljan, R. Sauleau, and M. Albani, "Efficient analysis of lossy substrate integrated waveguide structures," *IEEE Int. Antennas and Propag. Symposium*, 6-11 Jul. 2014, Memphis, TN, USA.

[27] M. A. Leontovich, "Approximate boundary conditions for electromagnetic field on the surface of conducting bodies," in *Collection Book Investigation of Radio Waves Propagation* (in Russian). Moscow, Russia: Academy of Sciences, 1948.

[28] L. B. Felsen and N. Marcuvitz, *Radiation and Scattering of Waves*. IEEE Press, 1994.

[29] R. E. Matick, Transmission Lines for Digital and Communication Networks. New York: McGraw-Hill, 1969.

[30] S. P. Morgan, Jr., "Effects of surface roughness on eddy current losses at microwave frequencies," *J. Appl. Phys.*, vol. 20, pp. 352–362, 1949.

[31] L. Tsang, X. Gu, and H. Braunisch, "Effects of random rough surface on absorption by conductors at microwave frequencies," *IEEE Microw. and Wireless Comp. Letters*, vol. 16, no. 4, pp. 221 – 223, Apr. 2006.

[32] R. Sorrentino, "Transverse resonance technique," in *Numerical Techniques for Microwave and Millimeter-Wave Passive Structures.* T. Itoh, Eds. New York: Wiley, 1989.

[33] G.W. Hanson, A.B. Yakovlev, *Operator Theory for Electromagnetics: An Introduction*. Springer, 2002.

[34] A. Valero-Nogueira, J.I. Herranz-Herruzo, E. Antonino-Daviu, and M. Cabedo-Fabres, "Evaluation of the input impedance of a top-loaded monopole in a parallel-plate waveguide by the MoM/Green's function method," *IEEE Transactions on Microwave Theory and Techniques*, Vol. 53, No. 3, pp. 868-873, March 2005.

[35] U. Rosenberg, M. Salehi, J. Bornemann, and E. Mehrshahi, "A novel frequency-selective power combiner/divider in single-layer substrate integrated waveguide technology," *IEEE Microw. Wirel. Comp. Lett*., vol. 23, no. 8, pp. 406 – 408, Aug. 2013.

[36] H. Ikeuchi, I. Ohta, M. Kishihara, and T. Kawai, "Honeycomb substrate integrated waveguide (HCSIW) and its application to design of SIW right-angle corner," *Proceedings of the 42nd European Microwave Conference*, Amsterdam (Nederland), Oct. 29 - Nov. 1 2012.

[37] L.Szydlowski, N. Leszczynska, and M. Mrozowski, "A linear phase filter in quadruplet topology with frequency-dependent couplings," *IEEE Microw. Wirel. Comp. Lett*., vol. 24, no. 1, pp. 32 – 34, Jan. 2014.

[38] S. H. Han, X. L. Wang, Y. Fan, Z. Q. Yang, and Z. N. He, "The generalized Chebyshev substrate integrated waveguide diplexer," *Progress In Electromagnetics Research*, PIER 73, pp. 29–38, 2007.

Massimiliano Casaletti (M'10) was born in Siena, Italy, in 1975. He received the Laurea degree in telecommunications engineering and the Ph.D. degree in information engineering from the University of Siena, Siena, Italy, in 2003 and 2007, respectively.

From 2003 to 2005, he was with the Research Center MOTHESIM, Les Plessis Robinson, Paris, France, under EU grant RTN-AMPER (RTN: Research Training Network, AMPER: Application of Multiparameter Polarimetry). He worked as a Research Associate with the University of Siena from 2006 to 2010, and a Postdoctoral Researcher from 2010 to 2013 with the Institut d'Electronique et des Télécommunications de Rennes (IETR), University of Rennes 1, Rennes, France. He is currently an Associate Professor with the University Pierre et Marie Curie (UPMC), Paris, France. His research interests include numerical methods for electromagnetic (scattering, antennas, and microwave circuits), metasurface structures, field beam expansion methods, and electromagnetic band-gap structures.

Dr. Casaletti was the co-recipient of the Best Poster Paper Award at the 3rd European Conference on Antennas and Propagation (EuCAP-2009), Berlin, Germany, the Honorable Mention for Antenna Theory at EuCAP-2010, Barcelona, Spain, and the Best Paper Award on Antenna Theory at EuCAP-2011, Rome, Italy.

Guido Valerio (S'06–M'10) received the M.S. degree (cum laude and honorable mention) in electronic engineering in 2005, and the Ph.D. degree in electromagnetics in 2009, from La Sapienza University, Rome, Italy. From February to August 2008 he was a Visiting Scholar at the University of Houston, TX, USA. From 2011 to 2014, he was a researcher at the Institute d'Electronique et de Telecommunications de Rennes (IETR), France. Since September 2014 he is an Associate Professor in the Electronics and Electromagnetism Laboratory, at Sorbonne Universités, Université Pierre et Marie Curie, Paris, France.

His scientific interests involve numerical methods for wave propagation and scattering in complex structures; namely, efficient computation of periodic Green's functions, the interaction of nonperiodic sources with periodic media, modal properties of multilayered structures, full-wave methods for large multilayered SIW. He has worked in the GPR characterization of Martian soil, and in the design of UWB antennas, harmonic-tunable active antennas, leaky-wave antennas, multifunction antenna arrays.

In 2008 Dr. Valerio was the recipient of the "Leopold B. Felsen Award for Excellence in Electrodynamics." In 2009 he was a finalist for the "Young Engineering Prize" at the *European Microwave Conference*. In 2010 he was the recipient of the "Barzilai Prize" for the best paper at the *National Italian Congress of Electromagnetism* (*XVIII RiNEm*). In 2014, he was the recipient of the RMTG Award for junior researchers presented at the *IEEE Antennas and Propagation Society Symposium*, Memphis, TN.

Ronan Sauleau (M'04–SM'06) received the Degree in electrical engineering and radio communications from the Institut National des Sciences Appliquées, Rennes, France, in 1995, the Agrégation degree from the Ecole Normale Supérieure de Cachan, Cachan, France, in 1996, and the Ph.D. degree in signal processing and telecommunications and the Habilitation à Diriger des Recherches degree from the University of Rennes 1, Rennes, France, in 1999 and 2005, respectively.

He was an Assistant Professor and Associate Professor with the University of Rennes 1 from 2000 to 2005 and from 2005 to 2009, respectively. He has been a Full Professor with the University of Rennes 1 since 2009. He has shared the responsibility of the research activities on antennas with the Institute of Electronics and Telecommunications of Rennes (IETR), Rennes, in 2010 and 2011. He is currently the Co-Director of the Research Department Antenna and Microwave Devices at IETR, where he is also a Deputy Director. He has been involved in more than 35 research projects at the National and European levels and has co-supervised 20 post-doctoral fellows, 35 Ph.D. students, and 48 master's students. He holds ten patents. He has authored or coauthored over 190 journal papers and 400 publications in international conferences and workshops. His current research interests include numerical modeling (mainly FDTD), millimeter-wave printed and reconfigurable antennas, substrate integrated waveguide antennas (SIW), lens-based focusing devices, periodic and nonperiodic structures (electromagnetic bandgap materials, metamaterials, reflectarrays, and transmitarrays), and biological effects of millimeter waves.

Prof. Sauleau was elevated to Junior Member of the Institut Universitaire de France, Paris, France, in 2007. He was the recipient of the 2004 ISAP Conference Young Researcher Scientist Fellowship, Japan, and the first Young Researcher Prize in Brittany, France, in 2001, for his research work on gain-enhanced Fabry–Perot antennas. He was the recipient of the Bronze Medal by the CNRS in 2008. He was a corecipient of several international conference awards with some of his students (Int. Sch. of BioEM 2005, BEMS'2006, MRRS'2008, EMRS'2011, BEMS'2011, IMS'2012, Antem'2012, and BioEM'2015). He served as a Guest Editor for the IEEE TRANSACTIONS ON ANTENNAS AND PROPAGATION for the "Special Issue on Antennas and Propagation at Millimeter and Submillimeter-Waves."

Matteo Albani (M'98–SM'10) received the Laurea degree in electronic engineering and the Ph.D. degree in telecommunications engineering from the University of Florence, Florence, Italy, in 1994 and 1999, respectively.

Currently, he is an Associate Professor with the Department of Information Engineering and Mathematics, University of Siena, Siena, Italy, where he is also the Director of the Applied Electromagnetics Laboratory. From 2001 to 2005, he was an Assistant Professor with the University of Messina, Messina, Italy. He has coauthored more than 65 journal papers and more than 180 conference papers. His research interests include high-frequency methods for electromagnetic scattering and propagation, numerical methods for array antennas, antenna analysis and design, and metamaterials.

Dr. Albani is a member of EurAAP and URSI. He was the recipient of the "G. Barzilai" Young Researcher Best Paper Award at the XIV RiNEM, Ancona, Italy, in 2002, and the URSI Commission B Young Scientist Award at 2004 URSI EMTS, Pisa, Italy. He was a Coauthor and Advisor of the winners of the Best Paper Award at the First European AMTA Symposium 2006, Munich, Germany and of the "3rd Prize Young Scientist Best Paper Award" at 2010 URSI EMTS, Berlin, Germany. With his coauthors, he was awarded with the Antenna Theory Best Paper at the EuCAP 2014, den Haag, the Netherlands.